



HAL
open science

The “BOUSSOLE” buoy - A new transparent-to-swell taut mooring dedicated to marine optics: Design, tests, and performance at sea

David Antoine, Pierre Guevel, Jean-Francois Deste, Guislain Becu, Francis Louis, Alec J. Scott, Philippe Bardey

► To cite this version:

David Antoine, Pierre Guevel, Jean-Francois Deste, Guislain Becu, Francis Louis, et al.. The “BOUSSOLE” buoy - A new transparent-to-swell taut mooring dedicated to marine optics: Design, tests, and performance at sea. *Journal of Atmospheric and Oceanic Technology*, 2008, 25 (6), pp.968-989. 10.1175/2007JTECHO563.1 . hal-03494345

HAL Id: hal-03494345

<https://hal.science/hal-03494345>

Submitted on 24 Dec 2021

HAL is a multi-disciplinary open access archive for the deposit and dissemination of scientific research documents, whether they are published or not. The documents may come from teaching and research institutions in France or abroad, or from public or private research centers.

L’archive ouverte pluridisciplinaire **HAL**, est destinée au dépôt et à la diffusion de documents scientifiques de niveau recherche, publiés ou non, émanant des établissements d’enseignement et de recherche français ou étrangers, des laboratoires publics ou privés.



Distributed under a Creative Commons Attribution 4.0 International License

The “BOUSSOLE” Buoy—A New Transparent-to-Swell Taut Mooring Dedicated to Marine Optics: Design, Tests, and Performance at Sea

DAVID ANTOINE

Laboratoire d'Océanographie de Villefranche, CNRS-Université Pierre et Marie Curie, Paris, France

PIERRE GUEVEL AND JEAN-FRANÇOIS DESTÉ

ACRI-IN, Sophia Antipolis, France

GUISLAIN BÉCU*

Laboratoire d'Océanographie de Villefranche, CNRS-Université Pierre et Marie Curie, Paris, and ACRI-IN, Sophia Antipolis, France

FRANCIS LOUIS AND ALEC J. SCOTT⁺

Laboratoire d'Océanographie de Villefranche, CNRS-Université Pierre et Marie Curie, Paris, France

PHILIPPE BARDEY

ACRI-IN, Sophia Antipolis, France

(Manuscript received 28 March 2007, in final form 24 October 2007)

ABSTRACT

A new concept of oceanographic data buoy is described, which couples a taut mooring and a “transparent-to-swell” superstructure, and is specifically designed for the collection of radiometric quantities in offshore environments. The design of the thin superstructure addresses two major requirements: stabilizing the instruments in the water column and avoiding shading them. The development of the buoy is described, starting with the theoretical assessment and then describing the various stages of development leading to the latest version of the mooring and buoy. Its performance at sea is also analyzed. This new platform has been deployed in the deep waters (>2400 m) of the northwestern Mediterranean Sea for about 4 yr (since September 2003) and provides a quasi-continuous record of optical properties at this site. The data are used for bio-optics research and for calibration and validation operations of several European and U.S. ocean color satellite missions. The plan is to continue the deployment to build a decadal time series of optical properties. The instrument suite that is installed on this buoy is also briefly described, and sample results are shown to demonstrate the ability of this new system to collect the data at the desired frequency and quality.

1. Introduction

Optical remote sensing of the ocean, generally referred to as “ocean color remote sensing,” has greatly developed in the past decades since the proof-of-concept “Coastal Zone Color Scanner” (CZCS) was launched in November 1978 by the National Aeronautics and Space Administration (NASA; Hovis et al. 1980). The constellation of ocean color sensors that now exists thanks to the launch of various satellites by several space agencies provides a virtually daily cover-

* Current affiliation: GEMS Survey, Ltd., Devizes, Wiltshire, United Kingdom.

+ Current affiliation: Fugro GEOS, Ltd., Wallingford, Oxfordshire, United Kingdom.

Corresponding author address: D. Antoine, LOV, Caserne Nicolas, BP 8, 06238 Villefranche sur mer, France.
E-mail: antoine@obs-vlfr.fr

age of the ocean surface (Yoder 1999). The data provided by these sensors are useful for scientific research and a variety of operational applications, such as global carbon cycle research (McClain et al. 2006), assimilation into global circulation models (e.g., Natvik and Evensen 2003), fisheries regulation, and coastal zone monitoring and management (Sathyendranath 2000).

Before they become useful for such areas of application, the top-of-atmosphere (TOA) observations from these satellite sensors (i.e., the radiance backscattered by the earth's surface and atmosphere recorded in several finite spectral bands) have to be properly calibrated. Then the geophysical parameters that are subsequently derived from these TOA observations through a series of algorithms have to be validated against so-called sea truth data. The validation of data from several sensors against a unique set of in situ data is also a mandatory step before they can be merged, which is nowadays one of the major goals of the international ocean color community (e.g., Antoine 2004; Gregg 2007).

These two processes, calibration and validation, must be pursued throughout the life of an ocean color mission to permanently maintain the quality of the derived products at the desired level (e.g., Hooker and McClain 2000). An intensive field work is therefore needed for the collection of the relevant data. These data include in particular the water-leaving radiance, noted L_w , which is the primary quantity derived from the TOA satellite observations after the atmospheric effects are removed, and on which the derivation of all other quantities rely through various "bio-optical" algorithms (e.g., O'Reilly et al. 1998; Morel and Maritorena 2001). Water-leaving radiances must therefore be collected at sea, and stringent requirements are attached to the accuracy of such measurements (McClain et al. 1998).

Nowadays, a common way to collect these data is to use in-water profiling radiometers, commercially available from several companies. These instruments have slightly negative buoyancy and are equipped with stabilizing fins, so that they can freely and vertically sink within the water column, provided that the cable that physically connects them to the ship is kept loose. The instrument can also be deployed far enough from the ship so it is out of the ship-shaded area. Irradiance and radiance profiles are therefore obtained with a tilt angle usually $<5^\circ$. The water-leaving radiance is then determined through extrapolation of the top meters' measurements (see Hooker et al. 2001). In spite of their numerous advantages (simplicity of use, low tilt, low shading), such ship-based deployments inevitably end up with a very small number of good-quality in situ measurements collocated with clear-sky satellite obser-

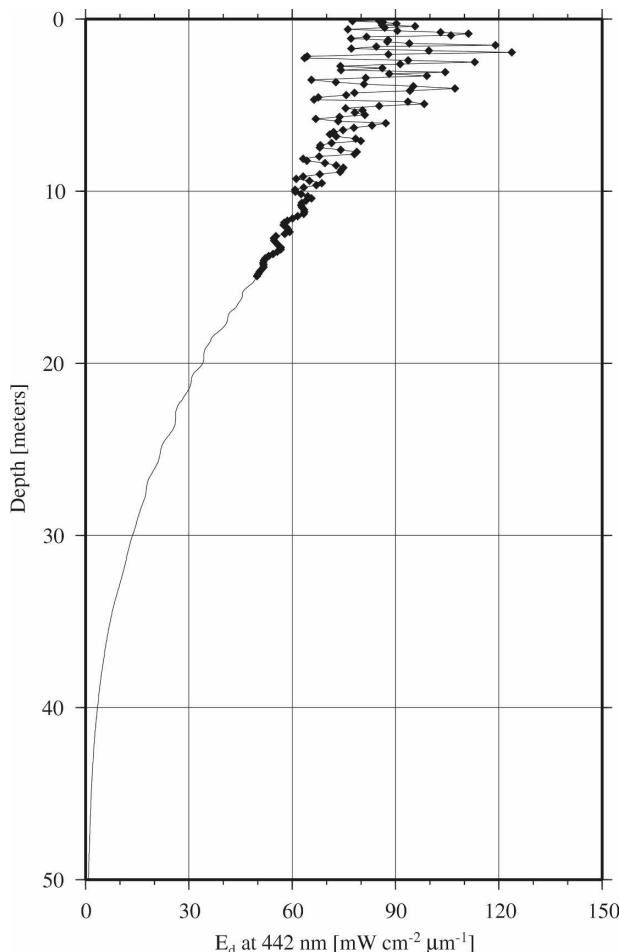


FIG. 1. Downward irradiance at 442 nm as a function of depth as measured at the deployment site at 1435 UTC 4 Jun 2004. The radiometer has a descent rate of about 0.8 m s^{-1} with a 6-Hz acquisition frequency.

vations. The reason for this is the long list of criteria that must be respected for a comparison point to be useful for validation purposes (e.g., Bailey and Werdell 2006). Circumventing this limitation needs a denser acquisition scenario, which is possible thanks to autonomous measurement platforms such as a fleet of autonomous underwater vehicles (e.g., Argo floats for physical information; Argo Science Team 1998), coastal platforms in shallow waters (e.g., Zibordi et al. 2002, 2006a), or moorings when the offshore environment is concerned. The technical realization that is developed in this paper corresponds to the second option.

A general difficulty in using radiometric data collected near the surface (i.e., depths shallower than about 20 m) comes from the fluctuations of radiance and irradiance generated by wave focusing (Fig. 1). These fluctuations exist as soon as capillary waves create some roughness, even without the presence of

swells (e.g., Dera and Gordon 1968; Stramska and Dickey 1998). The presence of swells adds variations of longer wavelengths that, combined with the fast small-scale fluctuations, create horizontal gradients in radiance and irradiance that are larger than the vertical change created by the logarithmic attenuation of radiation with depth. This contradicts the assumption of a horizontally homogeneous ocean, on which most of the approximations of radiative transfer are derived. A thorough review of the statistics of the light field variations caused by surface waves can be found in Walker (1994), and issues more specific to the measurement of radiance and irradiance in the context of ocean optics were recently analyzed in Zaneveld et al. (2001). There are several solutions to overcome this second limitation. The first one would be to average thousands of simultaneous measurements taken over “suitably large areas” (Zaneveld et al. 2001), which is obviously impracticable. Infinitely increasing the sampling rate and decreasing the drop rate would also reconcile the unique realization of a single irradiance profile with the large-scale irradiance profile; approaching this theoretical solution with slow drop rates is feasible, and has been experimentally investigated in coastal waters (Zibordi et al. 2004). The third solution is to continuously measure at a fixed depth with respect to ground during several of the typical time scales of the light field fluctuations, and then to apply some statistical treatment to the data (averaging, taking the median, filtering, etc.) to get the value that would be measured in the absence of such fluctuations. This third solution has been adopted here.

A successful example of a buoy dedicated to optics is the Marine Optical Buoy (MOBY; Clark et al. 1997, 2003) jointly developed by the National Oceanic and Atmospheric Administration (NOAA) and NASA in view of providing a mission lifetime record of the water-leaving radiance for the NASA Sea Viewing Wide Field of View Sensor aboard the Orbital Science Corporation (OSC) Orbview-II satellite (SeaWiFS mission; Hooker and Esaias 1993) and for the NASA Moderate Resolution Imaging Spectrometer aboard the NASA *Aqua* satellite (MODIS-A; Salomonson et al. 1992). This buoy has been operationally deployed since 1994 in the vicinity of Lanāi Island in the Hawaiian archipelago and has been the central element of the calibration and validation plan for these two missions. The MOBY design is adapted to an area protected from large swells and relatively easily reachable (15 n mi from coast), which is not the case in the present program (see later). Another example was the Plymbody buoy deployed during several months in the English Channel (Pinkerton and Aiken 1999). Other moorings

have hosted radiometers or active optical sensors (e.g., fluorometers), such as the Bermuda Test Bed Mooring (Dickey et al. 1998), but were not necessarily dedicated to providing data for validation purposes over the long term.

In the frame of the calibration and validation activities of the European Space Agency (ESA) Environmental Satellite (*Envisat*), a project was set up with the objective of establishing a time series of optical properties in oceanic waters to support the calibration and validation of the Medium Resolution Imaging Spectrometer (MERIS; Rast et al. 1999) ocean color sensor. The panorama of existing solutions showed a limited number of dedicated platforms and programs. It became obvious that a specific development was inescapable, because platforms (buoys) developed for various oceanographic purposes are rarely adapted to the deployment of radiometers at sea. Recording the light field within the ocean interior is difficult because of the reasons previously exposed. The instruments themselves and, more dramatically, the platforms on which they are installed, inevitably introduce perturbations (shadowing in particular). Other difficulties originate from the need to keep the instruments as horizontal as possible, because horizontal plane irradiance (cosine sensors) and radiance in a given direction (generally nadir) are the required measurements. The actual measurement depth is also difficult to accurately assess, because rapid vertical displacements of the instruments sometimes occur, which prevent any precise estimation of pressure.

Therefore, the present paper describes the various stages of development of a new oceanographic data buoy—the BOUSSOLE buoy—the design of which has been optimized for measurement of radiometric quantities at sea. The name is actually that of the overall project within which the buoy was developed, literally translated from French as the “buoy for the acquisition of a long-term optical time series” (“boussole” is the French word for “compass”). This activity is composed of three basic and complementary elements: (i) a monthly cruise program, (ii) a permanent optics mooring, and (iii) a coastal Aerosol Robotic Network (AERONET; Holben et al. 1998) station. Each of these three segments is designed to provide specific measurements of various parameters at different and complementary spatial and temporal scales. When combined together, they provide a comprehensive time series of near-surface (0–200 m) ocean and atmosphere inherent optical properties (IOPs) and apparent optical properties (AOPs) needed to accomplish in particular the calibration/validation objectives mentioned above (Antoine et al. 2006, 2008; Hooker et al. 2007).

The present paper is focused on the new buoy. It describes the overall process starting from the theoretical calculations and ending up with the final and operational version. The instrument suite that is presently installed on the buoy is briefly presented, and sample data are also shown to demonstrate the capability of the new platform.

The organization of the paper deliberately follows the chronology of the various steps that were needed to reach the final design and construction, which now allows a quasi-permanent data collection at the selected site in the Mediterranean Sea. Writing along these lines illustrates the successive steps, tests, and optimizations, also including the unavoidable difficulties and failures that pave the way of technological development.

2. Constraints to be taken into account

The data to be measured are the upward and downward plane irradiances, E_u and E_d , as well as the radiance upwelling from nadir L at several depths in the water column near the surface. Besides the accurate characterization of the instrument field of view, the important point here is to aim at the correct direction (i.e., nadir). When the downward irradiance is measured just above the sea surface, the symbol E_s is used. This value is used as a reference, allowing the changes in the in-water irradiances that are only due to changes in the incoming solar radiation to be corrected.

Getting accurate values of E_s and of E_u , E_d , and L_u (nadir) at several depths in the water column requires that a first category of constraints is respected. The first one is that the platform has to minimize shading of the instruments because we measure the light field in the ocean. Then, because we aim at plane irradiances or at radiance from nadir, the platform has to be as vertical and stable as possible. The tilt with respect to the local vertical and the orientation with respect to the sun must be known. The measurement of E_s has to be performed sufficiently far above the sea surface as to be out of influence of sea spray.

Then, environmental constraints specific to the deployment site are also to be considered (i.e., the water depth at the deployment site is 2440 m, with no significant changes due to tides). Swells there can be up to 8 m but are usually lower than 5 m, and currents are usually low ($<10 \text{ cm s}^{-1}$). This last peculiarity is due to the selected position being in the central area of the cyclonic circulation that characterizes the Ligurian Sea (Millot 1999). The northern branch of this circulation is the Ligurian Current, which manifests as a jet flowing close to the shore in the southwesterly direction, and that, in turn, establishes a front whose position varies

seasonally. The southern branch of the circulation is a northeasterly current north of the island of Corsica; the eastern part of the circulation is essentially imposed by the geometry of the basin. A map is shown in Fig. 2 to show that the deployment site is typical of a deep-ocean offshore (60 km from the coast) mooring site.

The knowledge of the wave characteristics was important in the design of the BOUSSOLE buoy. The information was taken from the data collected by the French weather forecast agency (Météo-France), which deployed an Oceanographic Data Acquisition System (ODAS)-type meteorological buoy 2 n mi from the BOUSSOLE site. The distribution of swell heights and swell periods is displayed in Fig. 3a, and the density plot of the wave characteristics (i.e., significant height versus period) is displayed in Fig. 3b. These characteristics allowed determination of the vertical attenuation profile of the effect of swells in order to select the appropriate depth for the main buoyancy of the platform.

3. The solution adopted: Principle, theoretical assessment, preliminary tests, and operational deployments

a. General concept

The principle of the adopted solution is that of a “reversed pendulum,” with Archimedes thrust replacing gravity. A large sphere is stabilized at a depth out of the effect of most swells, at the end of a neutrally buoyant cable extending down to the sea floor. This sphere creates the main buoyancy of the system. A rigid and tubular structure is fixed above the sphere, which hosts the instrumentation. The resulting thrust ensures the stability of the system, which is subject to very limited forces from the so-called transparent-to-swell superstructure. The idea is that the buoy should be as fixed as possible with respect to ground, and has minimum resistance to waves and currents passing through. The instruments should not follow the surface elevations but rather remain at a constant depth with respect to the average surface.

This is a taut mooring, definitely different from what is usually referred to as spar buoys (e.g., Graber et al. 2000), and with a much larger tension on the cable than other types of taut moorings, such as the standard ATLAS mooring used in the TOA array (Milburn et al. 1996). The dynamic changes in the tension on the mooring cable are very small.

The principle is sketched on Fig. 4. With no waves and currents, the platform is vertical and positioned at a given depth. A drag is generated when waves and currents pass through the structure, with the effect of tilting the buoy. This drag has to be minimized, while

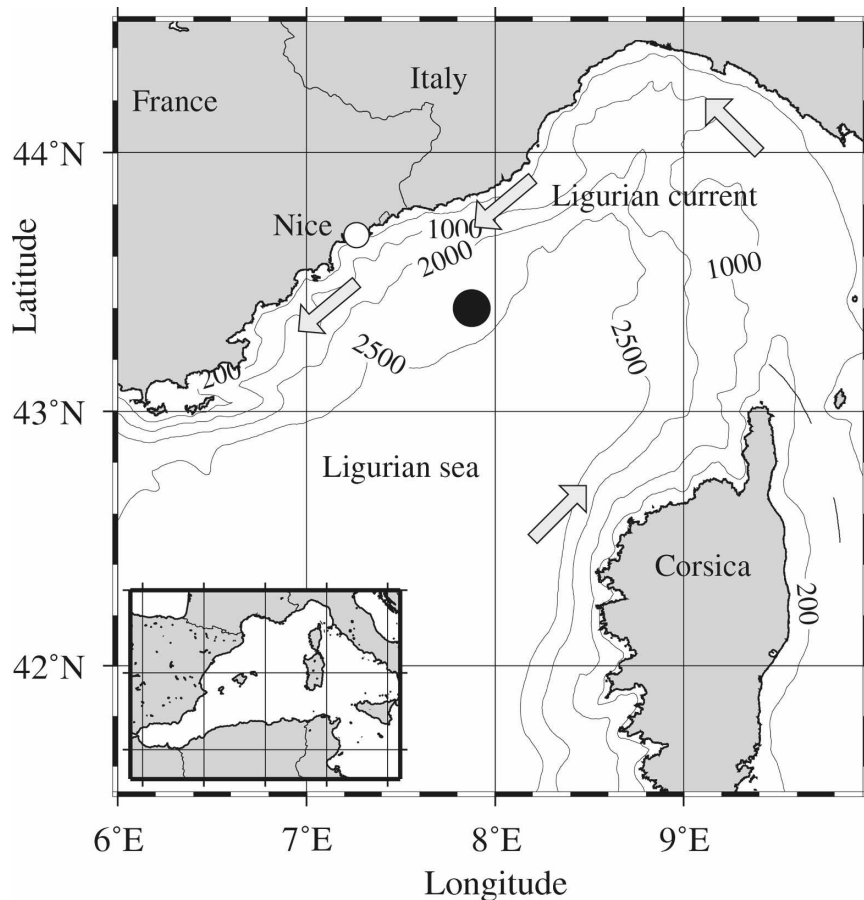


FIG. 2. The area of the northwestern Mediterranean Sea showing the southern coast of France and the island of Corsica plus the work area in the Ligurian Sea (black circle) for the BOUSSOLE activities. Gray arrows symbolize the main current branches.

the lift (righting torque) that will counterbalance the drag force has to be maximized. This equilibrium is obtained by minimization of the platform cross section and by an optimized repartition of weights and buoyancies. In terms of dynamics, motions are strongly reduced by viscous damping.

With such a design, there is no large body at the surface generating shade, and the underwater buoyancy sphere is far enough from the instruments that its effect on the underwater light field is negligible. With the final design (section 3e), the center of this sphere (diameter of approximately 2 m) is 8 m below the deepest radiometer (itself at 9 m), so that it only occupies about 0.05 sr within the upward hemisphere (i.e., about 1.5%). The impact on the measurement of the upward irradiance is therefore negligible. This sphere is out of sight of the radiance meters (half-angle is 10°), so that the measurement of the upwelling radiance is not affected either. The stability of the instruments is the other key characteristic of this new platform; it is war-

ranted even for quite large swells, and the possibility exists to accurately measure the water level above the instruments. Maintaining radiometers at a fixed depth and recording the light field during several minutes allows filtering of the fluctuations due to surface waves.

b. Theoretical assessment

Theoretical calculations were performed by specifying an initial and preliminary design and material for the construction (steel), and a swell of height 5 m and a period of 7 s, typical of the deployment site. The main characteristics of the initial and simplified design were, starting from the sea floor,

- a dead weight on the seafloor at 2350 m;
- a mooring cable of 2330 m, made of Kevlar (15-mm diameter, Young modulus 1.2×10^{11} N m⁻² or Pa, 0.22 m of elongation under a load of 1000 N);
- a lower tubular part, attached to the Kevlar cable;
- an empty sphere of diameter 1.6 m, placed at a depth of 18 m;

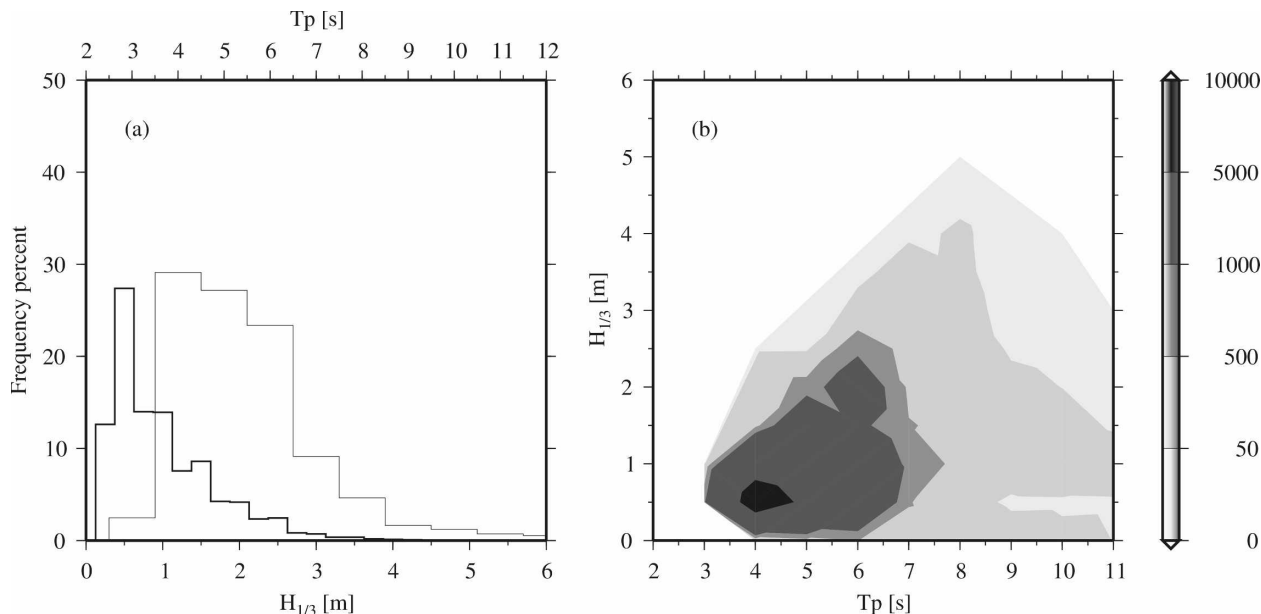


FIG. 3. (a) Histograms of the significant wave height ($H_{1/3}$; scale on the bottom axis; thick line) and of the wave period (scale on the top axis; thin line). Data are from 5 yr of measurements collected by the meteorological buoy deployed nearby the BOUSSOLE site by the French weather forecast agency (Météo France). (b) Significant wave height as a function of the wave period [same data as in (a)]. Note that an $H_{1/3}$ of 4 m, e.g., means a possibility of waves up to 6–8 m.

- an upper tubular part, made of four tubes of 9-m height and 0.1-m diameter, connected at their termination by a plate (the total weight of all the elements described above is 380 kg); and
- an upper superstructure of total height 12 m (with 3 m above the surface) and total weight 80 kg (with 10 kg on top to symbolize the aerial instrument package), made of four tubes of diameter 0.05 m, and connected to the plate of the lower tubular part.

Using these characteristics, the buoyancies (21 000 N for the whole system), inertia, righting torque, and generalized masses were determined. Then the natural response frequencies were calculated, as well as the period and amplitude of the oscillations and displacements due to swell and currents. These computations were following the simplified Froude–Krilov method and included the estimation of the viscous damping forces.

The natural response frequencies were found to be 92 s for surge, 2.6 s for heave, and 7.9 s for pitch. The magnitudes of oscillations were found to be ± 0.6 m for surge, ± 0.13 m for heave, and $\pm 1.9^\circ$ of tilt.

The system was also found to be quite sensitive to currents, with a tilt angle (in degrees) equal to $22 V_0^2$ and a horizontal displacement (in meters) of $92 V_0^2$, V_0 being the current speed at the sea surface (expressed in

meters per second), linearly decreasing to zero at the depth of the center of the buoyancy sphere.

Although the preliminary design was quite far from the final one, particularly regarding masses, these results were extremely encouraging in terms of tilt and oscillation, and demonstrated that the sensitivity to currents would require improvements. Among the possible solutions were increasing the diameter of the sphere, increasing the distance between the sphere and the attachment point to the cable, and minimizing the drag coefficient of the upper superstructure. Several series of calculations were performed with slightly different designs and with more realistic weights.

It was nevertheless decided to first build a reduced-scale model to perform tests in an engineering pool, with the aim of confirming the theoretical predictions and easily testing any modification of the design.

c. Tests of a reduced-scale model

A reduced-scale model (scale 1/10; see Fig. 5a) was built for the purpose of the verification of the theoretical predictions. The main floatation was represented by an empty sphere with walls made of synthetic foam, and all the tubular superstructures made of carbon fiber composite. Small brass masses were appropriately positioned to mimic the sizes and weights of the real instrumentation.

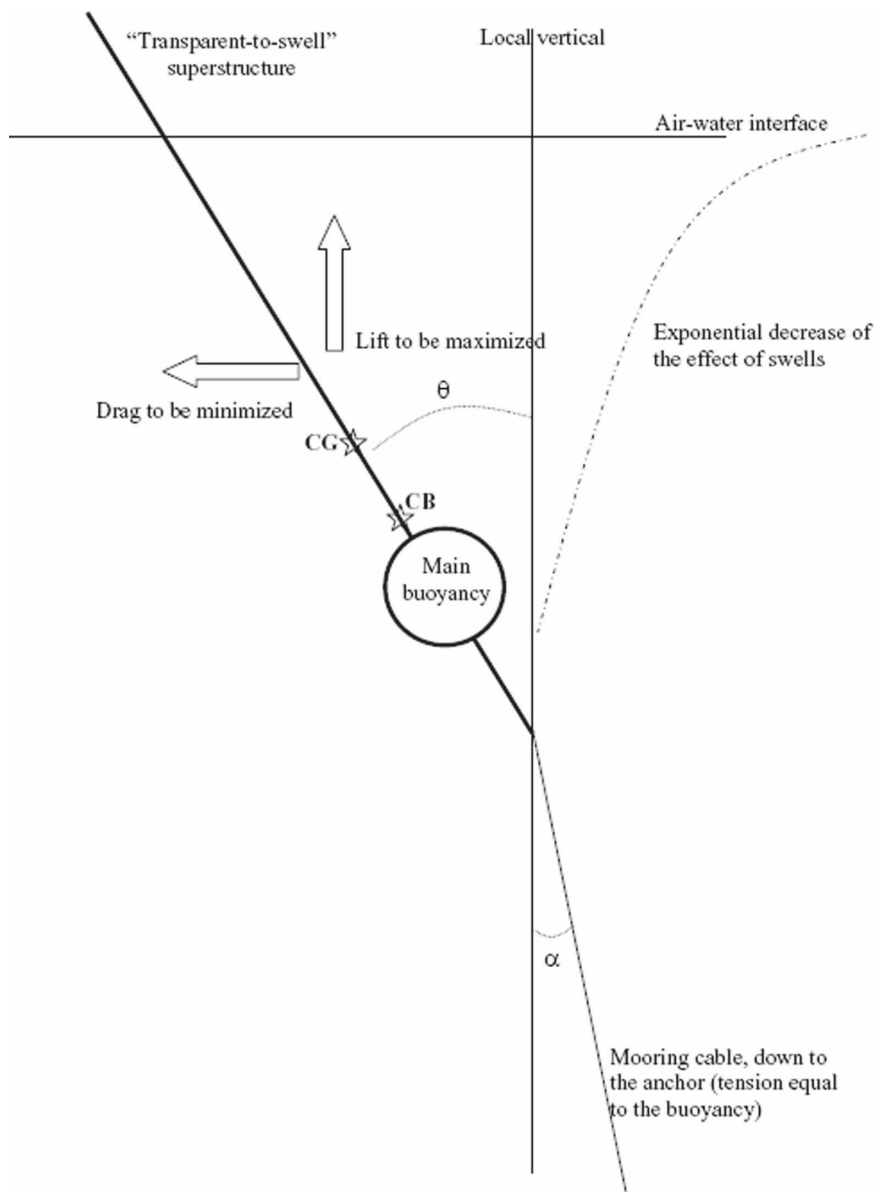


FIG. 4. Schematic of the basic principle of the BOUSSOLE buoy showing the main elements and driving forces. The buoy tilt and the angle of the mooring cable are exaggerated as compared to what they are in reality, just for the sake of clarity. In particular, the angle α is usually close to zero. The approximate positions of the center of gravity (CG) and of the center of buoyancy (CB) are also indicated by the two stars (see also Fig. 9).

The model was tested in an engineering pool of dimensions $24 \text{ m} \times 16 \text{ m} \times 3 \text{ m}$ with a 10-m central shaft (diameter of 5 m). The installation is shown in Fig. 5b. The mooring cable was simulated by a steel cable (diameter of 2 mm) terminated by an elastic, whose cross section was chosen so as to produce a stretch of $8.15 \times 10^{-3} \text{ m}$ when applying a force of 1 N. This assembly was mimicking the anticipated small elasticity of the Kevlar cable. The base of this pseudomooring was equipped

with a strain gauge, and the head of the reduced-scale model was equipped with four LED markers observed by a specific camera system. This system was able to describe motions and speeds in all directions. Monochromatic or random swells were applied, up to a 5-m real scale, and current was added in some cases.

The most significant results of these tests are shown in Fig. 6. They fully confirmed the theoretical predictions that were previously carried out, in terms of hori-

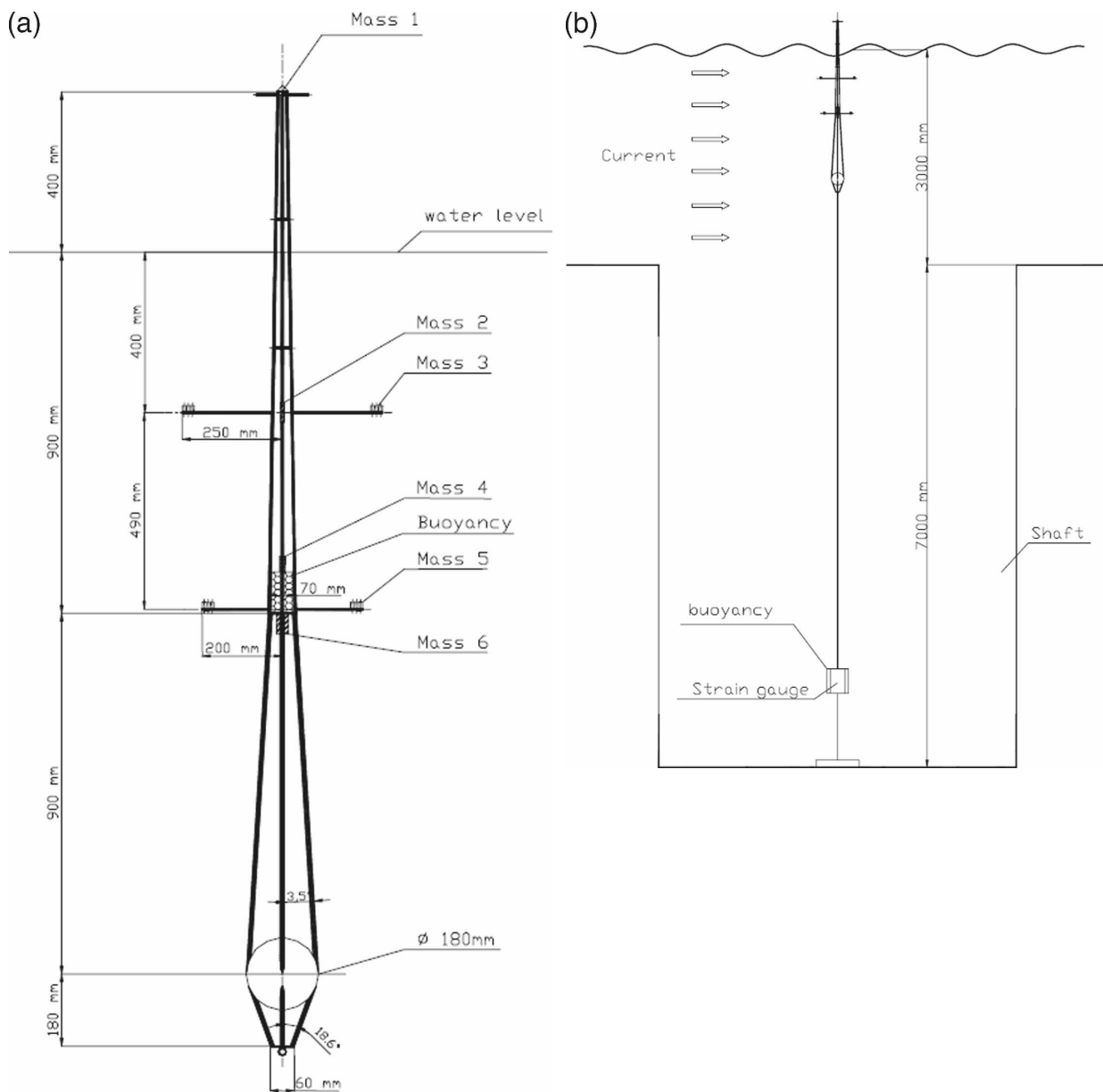


FIG. 5. (a) Sketch of the reduced-scale (1/10) model used for tests in the *Oceanide BGO First* engineering pool. (b) General organization of the reduced-scale model installation within the basin.

zontal and vertical displacements (the latter are extremely low), as well as in terms of angular deviations from the vertical. For instance, the mean tilt of the buoy is $\sim 4^\circ$ (with $\pm \sim 4^\circ$ of pitching) for a 4.6-m swell of period 5.2 s (i.e., at the limit before breaking occurs).

These tests also confirmed that no “hidden defect” (barely discernible via calculations only) was compromising the feasibility of the system. They also confirmed a significant sensitivity to currents, which are, however, low at the deployment site.

The tests fully supported the use of the adopted de-

sign, and led to the decision of building a first full-scale version of the buoy to perform a qualification deployment, which is described in the following section.

d. Version 1: Qualification deployment

The full-scale version 1 of the buoy was built in spring 2000. To minimize its weight, it was built of aluminum. It was made of two parts, the lower one that is from -20 to -9 m below the surface and consists of the sphere and a simple tubular structure, and the upper one that goes from -9 m below the surface to $+4.5$ m

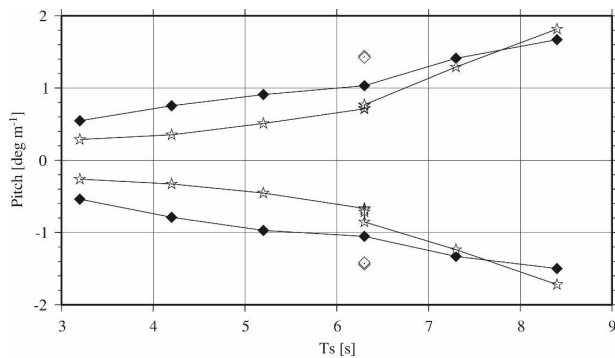


FIG. 6. Buoy pitch, expressed in degrees per meter of swell, as a function of the swell period. The black diamonds are for regular swells up to 4.6 m at full scale, the stars are for irregular waves up to 2.6 m at full scale. The open diamonds are for a regular swell with a period of 6.2 s plus a current of 0.5 m s^{-1} .

above the surface, and hosts the instrumentation. The details of the construction are not given here because it would be somewhat out of scope and because the subsequent versions of the buoy have been built differently (the nonoptimal characteristics of the construction of version 1 having been subsequently identified). It was not the purpose of this first version to make long-term deployments.

This version 1 was deployed on site during 3 months (20 July–20 October 2000), which allowed exposure to a variety of meteorological situations. The buoy was equipped with two inclinometers, a pressure sensor, an Argos beacon, and a flashing light. The goal of this deployment was to qualify the new concept of the buoy as well as to identify possible problems requiring modifications. A full day was required for the completion of the deployment operations, which were also totally new with respect to more classical oceanographic moorings. The details of these operations are provided in the appendix, along with the design of the complete mooring line in its final version.

The results of this deployment are shown in Figs. 7 and 8. Without entering into out-of-scope details, the following comments can be made (refer to the figure legends):

- The weather conditions during the 3 months are relatively stable, with slightly increased winds and waves in the last third of the record.
- Until mid-September, the periods where the buoy was tilted at angles larger than 5° were short, which means that version 1 already satisfied the requirements for meteorological conditions from calm to moderate.
- The behavior of the buoy progressively deteriorated after day 50 (Fig. 8), the reason being most certainly

higher current speeds (no measurement available, however), more frequent high wind speeds, and, finally, maybe some physical deterioration of the buoy itself.

- Oscillations were observed, which match the inertial period of the ocean at the latitude of the site [$12/\sin(\phi)$, expressed in hours], due to relaxation of the wind stress.
- A dramatic change of the buoy behavior started around day 63, which was not totally understood because the weather conditions were not so different before and after, except for the windstorm on days 64–65. When this record was retrospectively analyzed following the failure of the subsequent deployment (not detailed here), it was suspected that a leakage problem in the main buoyancy sphere actually started during the last phase of the qualification deployment.

In summary, the results of the qualification deployment were conclusive as to the feasibility of the new concept, but showed also a certain lack of righting torque, with consequences on the behavior of the buoy when the swell became greater than about 2 m. Although not dramatic, this behavior was not totally satisfactory. Therefore, some modifications in the design and construction of the buoy were introduced to improve the percentage of time that the inclination requirements would be satisfied. Several versions and deployments were needed to reach a satisfactory solution (including the loss of the buoy at deployment 2 because of a failure of the main buoyancy). Two additional and independent engineering studies were also performed with the aim of improving confidence in the design of the buoy and providing advice for better construction. They were conducted by the Institut Français de Recherche pour l'Exploitation de la Mer (IFREMER; LeBoulluec et al. 2002) and a Norwegian company specializing in offshore technology (MARINTEK; Hellan et al. 2002). Using their own tools, they made a critical assessment of what was done before, including the theoretical calculations and the implementations. The two studies eventually confirmed the feasibility and pertinence of the new concept. They also recommended using either foams or steel for the construction of the main buoyancy compartment. The second option was retained and a special design was prepared, which is now described.

e. The latest design

The main characteristics of the latest design (Fig. 9) are 1) the lower superstructure is made of steel (total

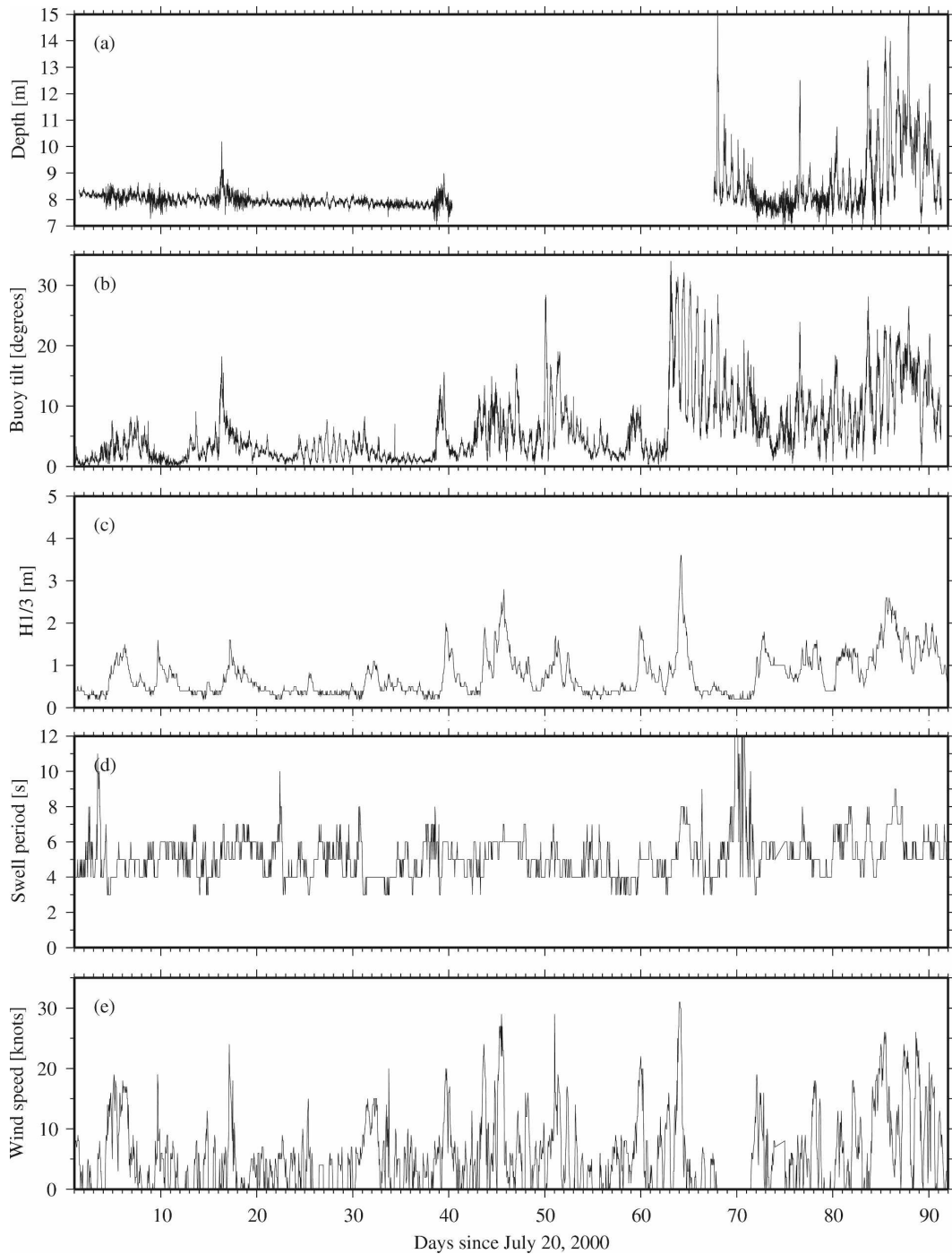


FIG. 7. The results of the qualification deployment (20 Jul–20 Oct 2000) showing the time series of (a) the depth of the buoy CTD (was nominally at 8.3 m when the buoy was motionless and the sea surface perfectly flat; interruption of the data stream is due to the failure of the battery), (b) the buoy tilt, (c) the swell height (the one-third most significant waves), (d) the swell period, and (e) the wind speed.

weight about 1300 kg), 2) the main buoyancy includes a cylindrical part, so that it is no longer a sphere but has some ovoid shape (to compensate for a larger weight), 3) the main buoyancy is segmented into seven pressure-

resistant and watertight compartments (see also Fig. 10) to minimize the risk of rapidly losing a large part of the buoyancy if a leakage was to occur, 4) the upper superstructure is made of aluminum (total weight about

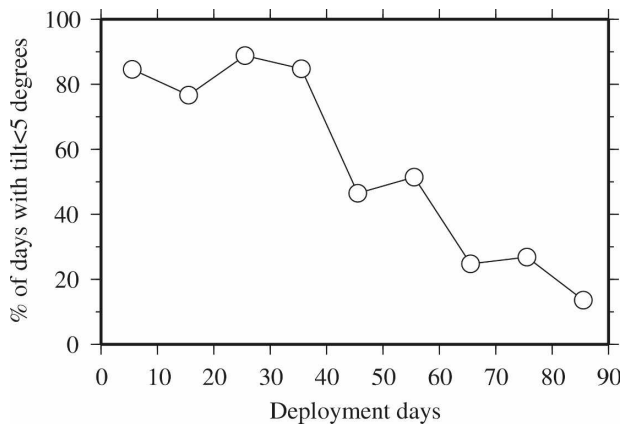


FIG. 8. The percentage of the tilt measurements that were less than 5° as computed over successive 10-day periods of the qualification deployment (conditions shown in Fig. 7).

200 kg), and 5) the distance between the center of the sphere and the cable is increased to 2.8 m.

In addition, a strain gauge was installed at the base of the buoy, just at the start of the mooring cable. Because the tension in the cable that is recorded by the gauge is, by definition, equal to the buoyancy of the entire mooring, any change in this buoyancy can be immediately detected.

This new buoy was deployed on 6 September 2003, and the upper instrumented part was recovered 3 months later on 6 December 2003. This recovery date was scheduled to avoid exposure of the buoy to the most hazardous weather season.

The behavior of the buoy was as expected, and the data collection was continuously operating during the 3 months. Images of the various stages of the deployment, and of the buoy itself taken from above and below water, are displayed in Fig. 10 to provide some practical feeling for what the complete system looks like.

During this deployment period, we experienced several storms, one with 45 kt of established wind speed and gusts up to 60 kt; maximum waves were about 7 m (this never occurred in the previous 5 yr). In such conditions, the strong wind-driven surface current pushes the buoy, which starts to tilt and simultaneously deepens because the Kevlar mooring cable cannot elongate. Therefore, after several hours of strong wind, the buoy simply becomes totally submerged, with the buoy head reaching maximum depths of about 8 or 10 m. This situation is not risky for the instrumentation, which is designed to go even deeper, and in some respects, it provides a good protection for the buoy from breaking waves, which are actually the only potential source of major damage to such a system. After the wind and the

current stop, the buoy quite rapidly goes back to its nominal position. This behavior is illustrated in Fig. 11, where a 7-day record of meteorological conditions and buoy tilt and depth is shown. The maximum tilt and deepening of the buoy occur about 1 day after the maximum wind and waves, and come back to equilibrium value after about 2 days. Besides such extreme situations, more “nominal storms” would not push the buoy head below water, and the equilibrium depth and tilt would be recovered within less than 12 h.

Another important characteristic of the BOUSSOLE mooring is the very small dynamic change in the tension of the cable, which guarantees its longevity by preventing it from suffering the abrupt application of large forces (“jerking”). This stability is the result of combining a large static tension ($\sim 28\,000$ N for the latest version) with a low forcing from the superstructure. An example is shown in Fig. 12, where the strain of the mooring cable is displayed along with the significant wave height and buoy depth. The strain record shown here is short and does not cover all the weather conditions that the mooring has experienced. The example of Fig. 12, nevertheless, includes a maximum significant wave height of 1.7 m, which corresponds to maximum waves of up to about 3 m. The changes in the tension of the cable during this 16-day record are of about 400 N peak to peak (i.e., less than 2% of the average static tension) and they do not show any significant increase when the larger waves are passing through the superstructure (10 June). The time lag between peaks is approximately corresponding to the inertial period at the latitude of BOUSSOLE.

After the initial 3-month deployment, the upper superstructure was reinstalled on 4 March 2004, and since then a mooring has been permanently on site collecting data. To ensure this quasi-permanent data acquisition, two entire mooring lines, buoys, and instrument suites have been built and assembled, allowing rotations on site to be performed about every 6 months. Replacement of the full mooring line, which is dictated by the need for replacing the Kevlar cable, is only performed about every 2 yr.

During the 3 yr of deployment between September 2003 and September 2006, the behavior of the buoy was in agreement with the theoretical calculations in terms of the relationship between the buoy tilt and depth (Fig. 13a). The cumulative histogram in Fig. 13b shows that 85% of the buoy tilts are $<10^\circ$. Considering the angular structure of the upward light field (e.g., Morel and Gentili 1993), a 10° tilt represents an uncertainty of less than 3% in the measurement of the upwelling nadir radiance, whatever the wavelength, except in the clearest waters ($\text{Chl} < 0.05 \text{ mg m}^{-3}$) when the difference

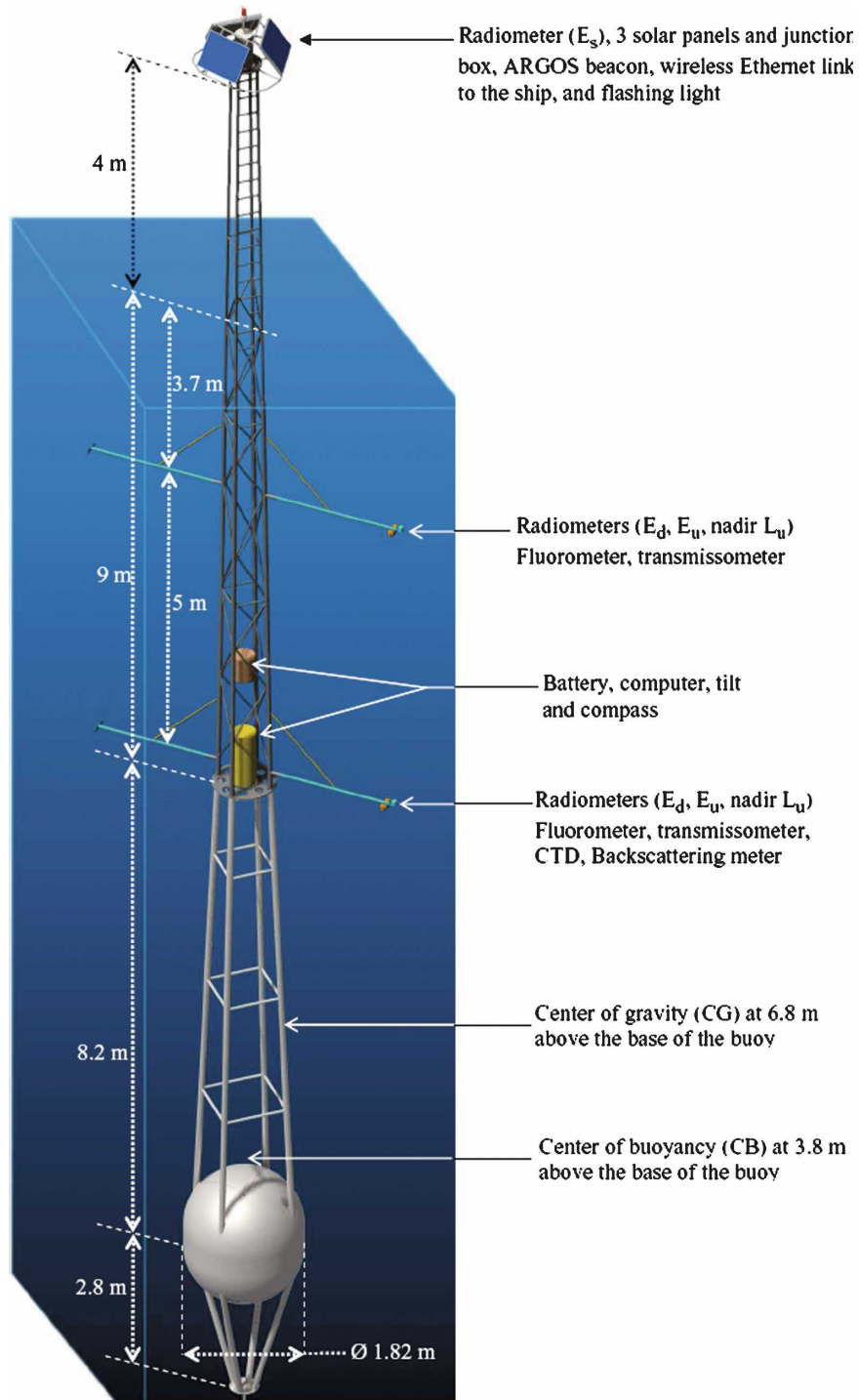


FIG. 9. Perspective “artist view” of the latest version of the BOUSSOLE buoy, showing the main dimensions and the location of instrumentation, as well as the position of the center of gravity (CG) and of the center of buoyancy (CB).

between the sun and the viewing azimuths is larger than $\sim 130^\circ$ or lower than $\sim 50^\circ$ (slightly depending on the solar zenith angle and the wavelength). In those conditions, the uncertainty can reach 5%. Conversely, buoy

tilts lower than 5° induce a less than 2% uncertainty on the measurement of the upwelling nadir radiance. A small bias of about 2° is observed in Fig. 13. It is actually due to an imperfect mass repartition in the lower

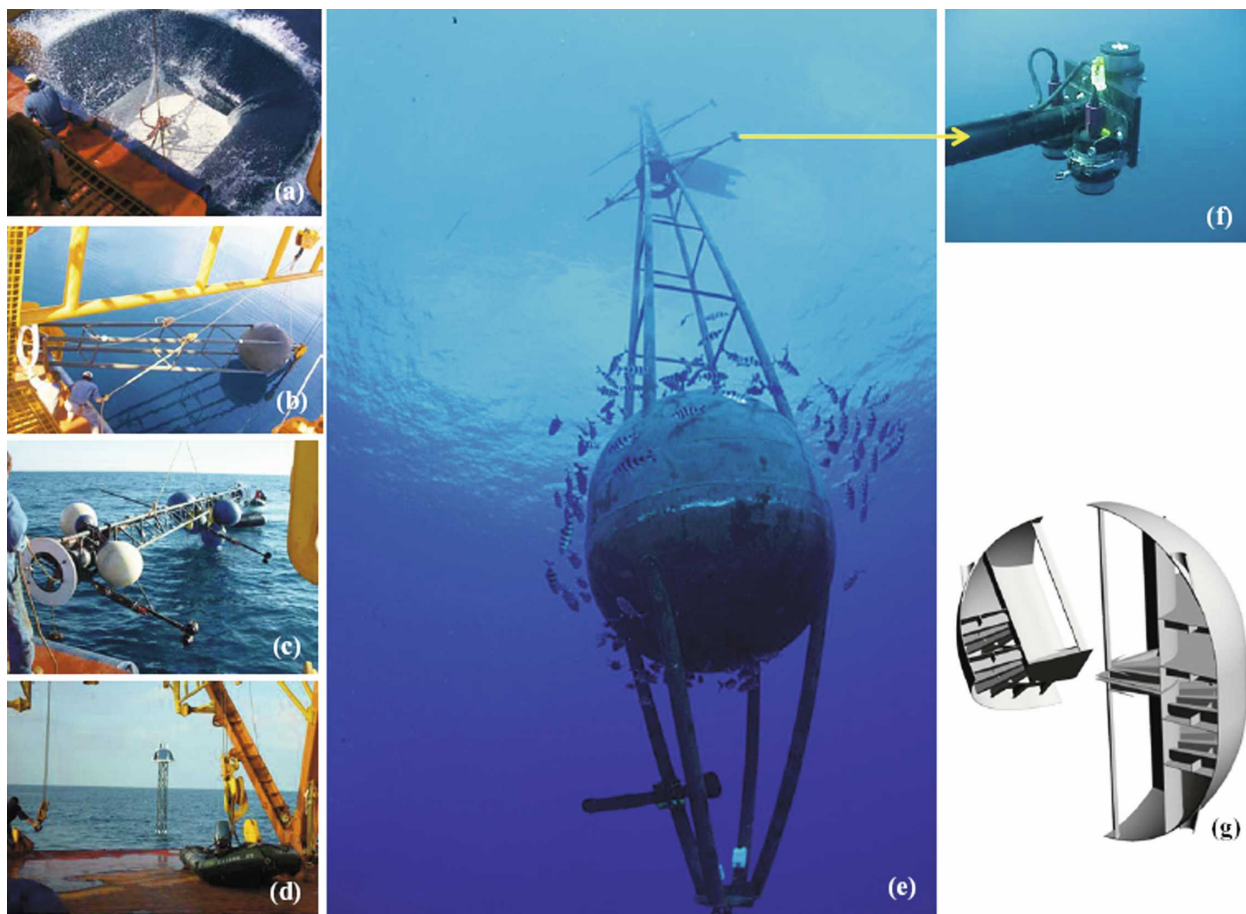


FIG. 10. Pictures taken on site at various stages of deployment of the buoy (note that this figure includes pictures taken from different versions of the buoy). (a) Drop of the dead weight after the entire mooring line has been laid at the sea surface; (b) progressive lowering of the main buoyancy sphere (ballast not yet installed on this picture); (c) deployment of the upper superstructure, hosting the instrumentation; (d) the buoy as it looks after deployment is achieved; (e) below-water image taken from the base of the buoy at 20-m depth, when the water was exceptionally clear (15 Mar 2006); the small dive boat is seen at the surface; (f) a zoom on the three radiometers installed at the end of the 9-m arm; and (g) layout of the seven pressure-resistant and watertight compartments within the main buoyancy sphere.

buoy superstructure, which ends up with a small 2° tilt when no forces are applied to the buoy.

4. Instrumentation and sample results

a. Sensors and data collection scenario

The buoy instrument suite is described in Table 1. These simultaneously collect data every 15 min. Each of the measurement sequence lasts 1 min, during which each instrument collects data at its own acquisition frequency.

The central recording component of the buoy is the Data Acquisition and Control Network (DACNet) unit, which houses the primary computer: a PC104 Cool RoadRunner II 200 MHz 6×86 with 32 MB of random

access memory (RAM) and the serial data acquisition equipment (recording to a 2-GB disk drive). These components are used in the collection, storage, and downloading of the data obtained from the instruments. Most of the time the system is inactive, and the DACNet unit is unpowered. A small internal microcontroller is responsible for the power supervision and control and a precision clock.

Optimization of the power budget is an important element, because of the restricted power available from the 12-Vdc 105-Ah underwater battery, which is recharged using three 40-W solar panels. The power management functions can be summarized as follows: 1) an accurate real-time clock, 2) an alarm clock for powering up the system for the programmed schedule, 3) a watchdog timer that protects against draining the battery in

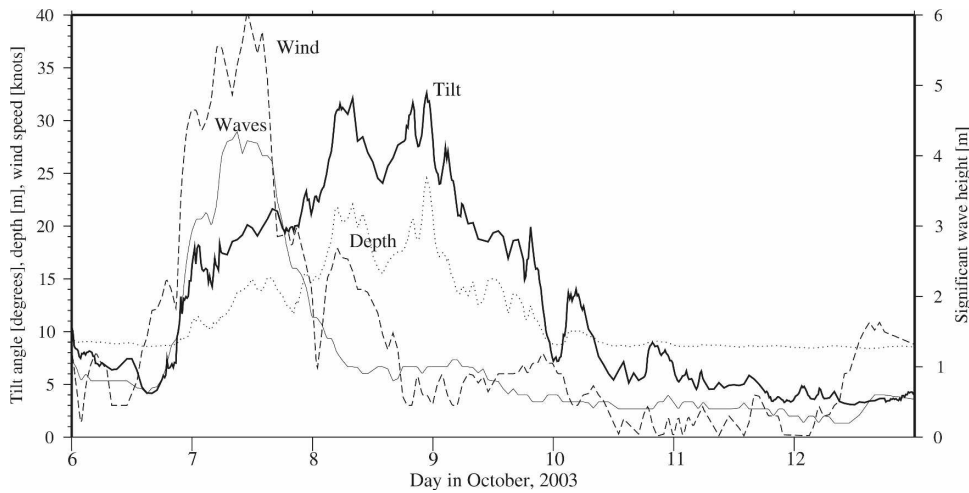


FIG. 11. Seven-day record of the buoy tilt (thick solid curve), buoy depth (dotted curve), wind speed (dashed curve), and wave height (thin solid curve) from 6 to 13 Oct 2003.

the event of a computer malfunction, and 4) a power-fail shutdown to prevent computer startup if the battery power is too low.

The DACNet operating system runs on Red Hat Linux 6.2-kernel v2.2.19, which accommodates custom-made Java software: the Satlantic Telemetry Acquisition Manager (STAM) and the Satlantic Node Manager. These programs provide the operational, configuration, and interface requirements for the buoy to run autonomously and enable communication of files with the user.

A third piece of software, Satlantic Base Manager, runs on a personal computer (PC) equipped with the Windows operating system and provides the operator

with administrative tools—each with a graphical user interface (GUI). These tools enable the user to configure the Node Manager, transfer data and files, update the internal clock of the acquisition node, view data from specified instruments in real time, and completely shutdown the acquisition node for maintenance.

The complete data stream can be downloaded through a wireless Ethernet link established between the buoy and the ship. This link functions with the ship positioned a few hundred meters from the buoy. The connection is driven by the buoy, with a wakeup sequence each hour of the day. This hierarchy was adopted, rather than establishing the communication from the ship, to minimize the time during which the

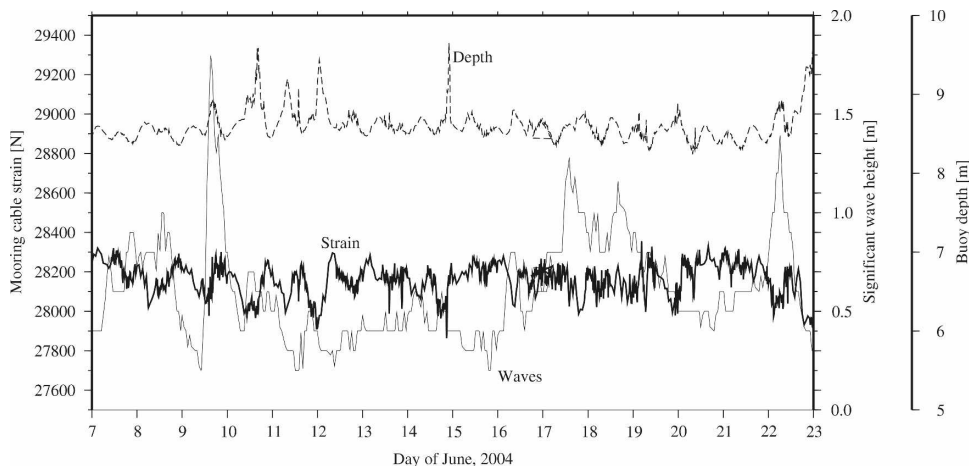


FIG. 12. Sixteen-day record of the strain of the mooring cable (thick solid curve), of the significant wave height (thin solid curve), and of the buoy depth, i.e., the pressure measured by a sensor nominally installed at 8.7 m when the buoy is at equilibrium (dashed curve).

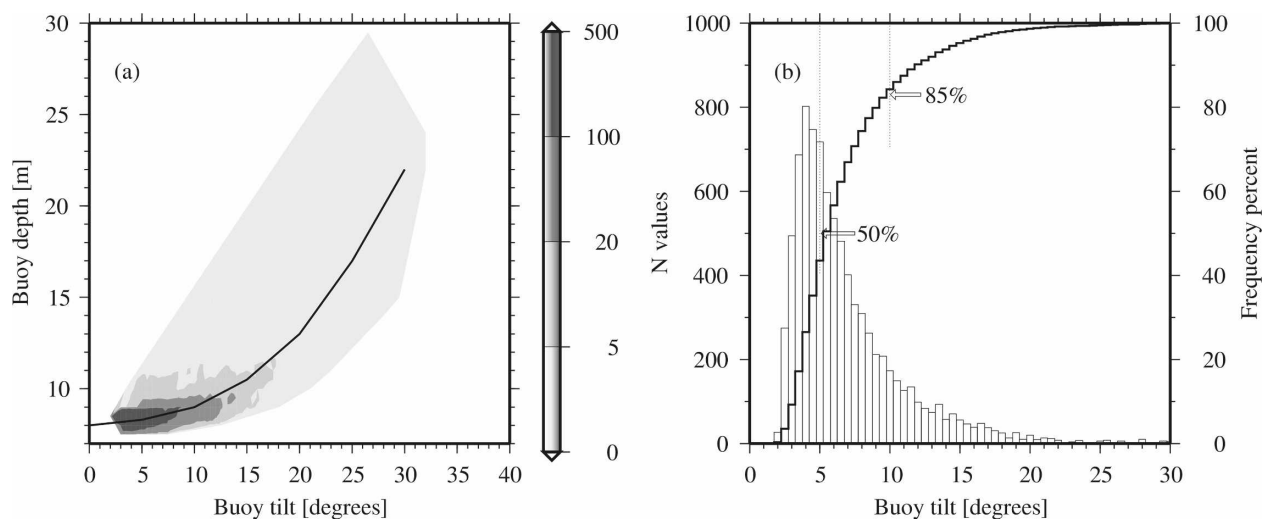


FIG. 13. (a) Buoy depth (i.e., depth of the pressure sensor, nominally at 8 m) as a function of the buoy tilt. The points are from the measurements collected from September 2003 to September 2006, and the curve is the theoretical prediction. (b) Histogram (left scale) and distribution function (right scale) of the buoy tilt, from the measurements shown in (a). The percentages of tilt values lower than 5° and 10° are indicated.

buoy communication hardware is awake and consuming energy.

Data retrieval from the buoy is performed from the DACNet via a Cisco Aironet 340 series wireless bridge

manufactured by Cisco Systems (San Jose, California) and is stored directly on a PC. The data are retrieved in a binary format and consist of one daily log file for each of the following seven groups: 1) the instruments con-

TABLE 1. Buoy instrument suite (December 2006).

Instrument type	Measured parameter(s)	Manufacturer	Model	Band set	Depth
Radiometers	E_d , E_u , and L_u at nadir	Satlantic Inc. (Halifax, Canada)	200 series OCR and OCI radiometers	412, 443, 490, 510, 560, 670, and 681nm (alternatively 412 is replaced by 555)	4 and 9 m
Radiometers	Above-surface E_s	As above	200 series MVDS	As above	+4.5 m
Compass and magnetometer	Two-axis tilt and compass	Advanced Orientation Systems, Inc. (Linden, New Jersey)	EZ-COMPASS-3A-DIVE	N/A	9 m
CTD	Conductivity, temperature, pressure	Sea-Bird Electronics (Bellevue, Washington)	37-SI CTD	N/A	9 m
Fluorometers	Phytoplankton chlorophyll fluorescence	Chelsea (Surrey, United Kingdom)	MINItracka Mk II	N/A	4 and 9 m
Transmissometers	Beam attenuation coefficient	Western Environmental Technology Laboratory (WETLabs) Inc. (Philomath, Oregon)	C-star	660 nm	4 and 9 m
Backscattering meter	Total volume scattering function at 140°	Hydro-Optics, Biology, and Instrumentation Laboratories (HOBI Laboratories), Inc. (Tucson, Arizona)	Hydroscat-II	442 and 560 nm	9 m

nected to the DATA-100 at 4 m (radiometers and fluorometers); 2) the instruments connected to the data acquisition module (DATA-100) at 9 m (radiometers, fluorometers, transmissometers); 3) the CTD; 4) the Hydrosat-II; 5) the strain gauge; 6) the Multichannel Visible Detector System (MVDS); and 7) the two-axis tilt sensor and compass. The daily file is closed once communication through the Cisco system occurs. In this case, a new file is created starting from the next measurement taken by the DACNet system until midnight or until a subsequent linkup via the Cisco system is performed. Storage space on the hard disk of the DACNet has the capacity to store up to approximately six months of data.

Part of the data stream is transmitted via the Argos system and is used for surveying the functioning of the system. The sample data include the tilt and depth of the buoy; the strain of the mooring cable, the battery voltage; the disk space; the spectrum of the above-water irradiance; and instrument health parameters, which indicate whether or not instruments and the acquisition system function nominally.

b. The parameters derived from the measurements and sample results

The set of parameters directly derived from the buoy above- and in-water measurements are as follows ($\lambda 7$ denotes the 7-channel spectral band set for the AOP sensors): 1) $E_s(\lambda 7)$; 2) $E_d(\lambda 7)$, $E_u(\lambda 7)$, $L_u(\lambda 7)$, $c(660)$, and chlorophyll fluorescence at 4 m; and 3) $E_d(\lambda 7)$, $E_u(\lambda 7)$, $L_u(\lambda 7)$, chlorophyll fluorescence, $c(660)$, $b_b(443)$, and $b_b(560)$, conductivity, temperature, pressure, and two-axis tilt and compass heading at 9 m. The wavelengths for the AOP measurements are 412, 443, 490, 510, 560, 665, and 683 nm (a spare set of sensors has the 412-nm channel replaced with 555 nm).

From these measurements, various AOPs or IOPs are derived: the diffuse attenuation coefficients for upward and downward irradiance K_u and K_d , the attenuation coefficient for upwelling radiance K_L , the diffuse reflectance just below the sea surface R , the nadir Q factor E_u/L_u , and the attenuation and backscattering coefficients c and b_b . Radiometry measurements are corrected for instrument self-shading as per Gordon and Ding (1992). The parameters entering into this correction are the instrument radius, which is 4.5 cm (common to all Satlantic 200-series radiometers), the total absorption coefficient, which is computed following Morel and Maritorena (2001) using the chlorophyll concentration, and the ratio between the direct-sun and diffuse-sky irradiances, which is computed following Gregg and Carder (1990) for a standard atmosphere [atmospheric pressure of 1013.25 hPa, ozone content of

350 DU, and a Shettle and Fenn (1979) maritime aerosol with an optical thickness of 0.2 at 550 nm]. There is no correction for possible residual shading by the buoy itself.

One important step of the data processing is a data reduction, which aims at producing one representative value for each of the 1-min sequences of acquisition. During these sequences, the radiometers collect about 360 measurements (acquisition rate of 6 Hz), which may include some outliers and are usually noisy because of the fluctuations of the radiative field due to the wave-roughened air-sea interface. This is illustrated in Fig. 14, where a sample acquisition sequence is represented, as a plot of the upward and downward irradiances as a function of time. The above-water irradiance was stable during this sequence, and the noise in the series is entirely due to the wave focusing effects. These effects are much larger for the downward flux than for the upward flux. Taking the median of the 360 measurements collected by the stabilized radiometers has been found to be a simple and robust way of filtering the data to get the value that would have been measured in the absence of perturbations from the interface. The design of the buoy, coupled to such a data filtering, allows irradiances to be measured near the surface.

Sample results are shown in Fig. 15 to illustrate the capability of the BOUSSOLE buoy. The data displayed in this figure correspond to all buoy measurements taken between 1000 and 1400 LT with a buoy tilt $<10^\circ$ and a buoy depth <11 m (black diamonds), onto which the MERIS-, SeaWiFS-, and MODIS-derived reflectances (red, blue, and green symbols, respectively) are superimposed. Interruptions of the in situ time series are due either to the absence of measurements or to the elimination of corrupted data (e.g., obvious instrumental problems). As for the satellite data, only those having met some quality criteria are plotted (see Bailey and Werdell 2006).

This analysis shows that the seasonal changes are well captured for all bands by the three sensors with no systematic seasonal bias. The dispersion of the satellite values is increasing for decreasing wavelengths. This is consistent with the known behavior of the atmospheric correction errors, which increase from the red to the blue (e.g., Gordon 1997).

When the satellite data are plotted against the buoy data, it is possible to evaluate the uncertainties and possible biases of the former ("match-up analysis"). A typical example is displayed in Fig. 16 for the MERIS sensor, using the same data as Fig. 15 and the match-up criteria proposed by Bailey and Werdell (2006). These results allowed identification of a bias in the MERIS

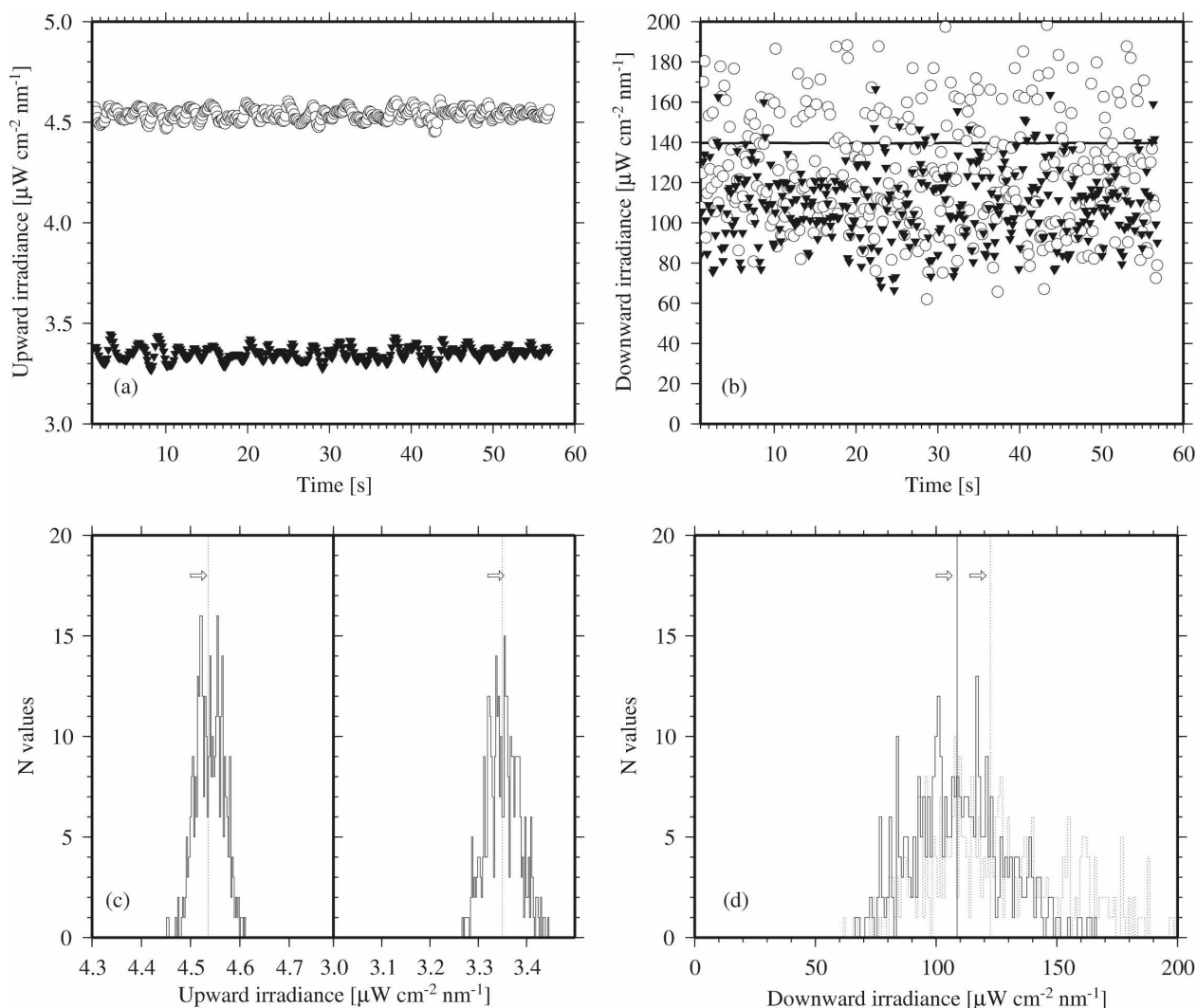


FIG. 14. A sample record of (a) upward and (b) downward irradiances at the two measurement depths, i.e., 4 and 9 m (open circles and black triangles, respectively), and for $\lambda = 490 \text{ nm}$. The above-water downward irradiance is also displayed in (b) (thick black line). (c), (d) The corresponding histograms are shown. The arrows indicate the median values of the distributions.

reflectance, in particular in the blue, as already pointed out by Zibordi et al. (2006b). Improvements of the atmospheric corrections as well as the introduction of a vicarious calibration were considered after this analysis was performed, showing the usefulness of such data.

More quantitative and in-depth analyses are out of scope here. The data shown here represent a unique record of the ocean reflectance in the Mediterranean Sea and, more generally, the product of a unique realization.

5. Conclusions

A new platform has been designed, which respects a list of requirements attached to the measurement of

radiometric quantities at sea. The final version of this buoy has been deployed for about 4 yr in the Mediterranean Sea and was still collecting data at the time this paper was written. The aim is to maintain a fully operational system throughout the coming years to build a decadal time series of optical properties at the BOUSSE site.

The data collected are now used for the calibration and validation operations for the three satellite ocean color sensors previously mentioned (i.e., the MERIS, SeaWiFS, MODIS-A, and also for the third Polarization and Directionality of the Earth Reflectance (POLDER-3) sensor aboard the *Polarization et Anisotropie des Réflectances au sommet de l'Atmosphère, couplées avec un Satellite d'Observation*

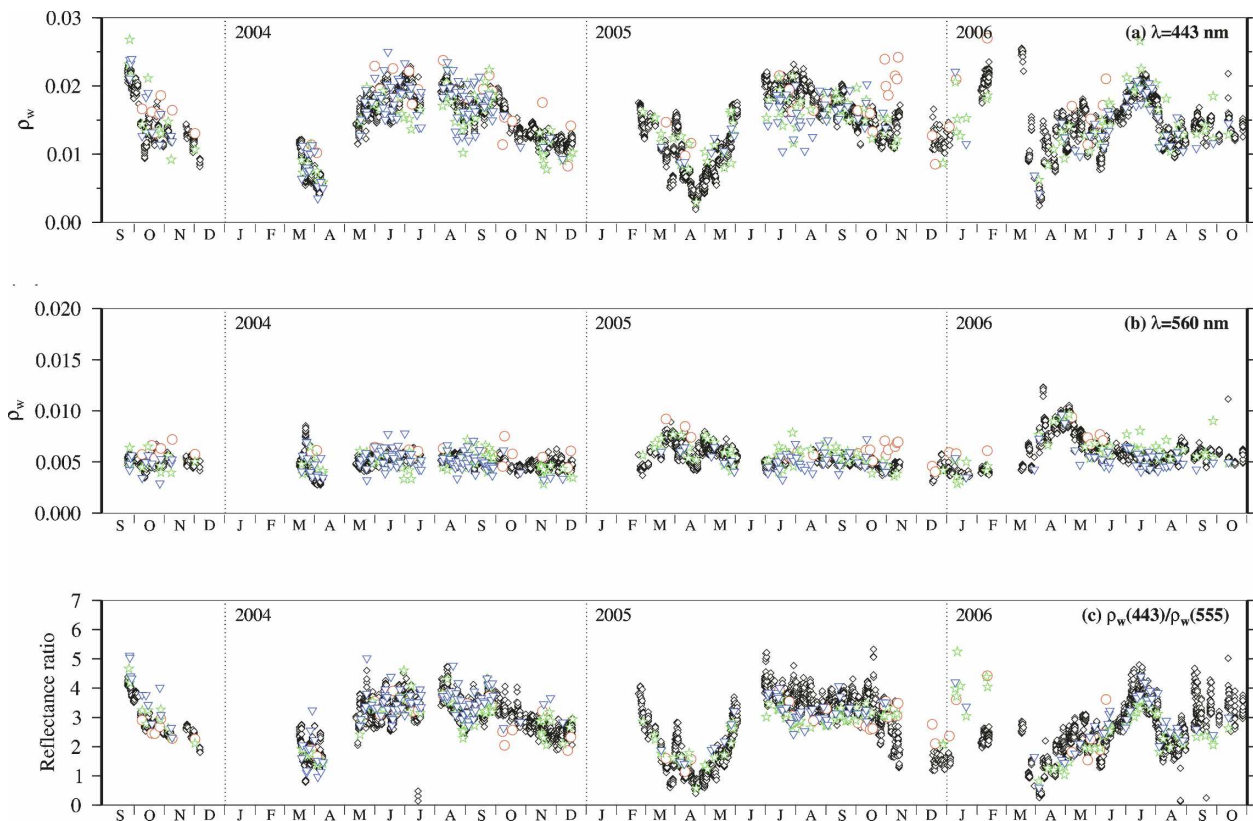


FIG. 15. Sample data collected by the BOUSSOLE buoy: (a) water-leaving reflectance, i.e., π times the ratio of the water-leaving radiance to the downward irradiance just above the sea surface at 443 nm [$\rho_w(443)$]; (b) the same quantity at another wavelength (560 nm); and (c) the ratio of $\rho_w(443)$ to $\rho_w(560)$, often used to determine the concentration of the phytoplankton chlorophyll-*a* in the upper layers (e.g., O’Reilly et al. 1998; Morel and Maritorena 2001).

emportant un lidar (PARASOL) satellite, from the French Centre National d’Etudes Spatiales (CNES). The data collected in the coming years might serve these objectives for future missions such as the NOAA-

NASA National Polar-orbiting Operational Environmental Satellite System/Visible Infrared Imaging Radiometer (NPOESS/VIIRS; Murphy et al. 2006) or the ESA Sentinel-3 (Drinkwater et al. 2005).

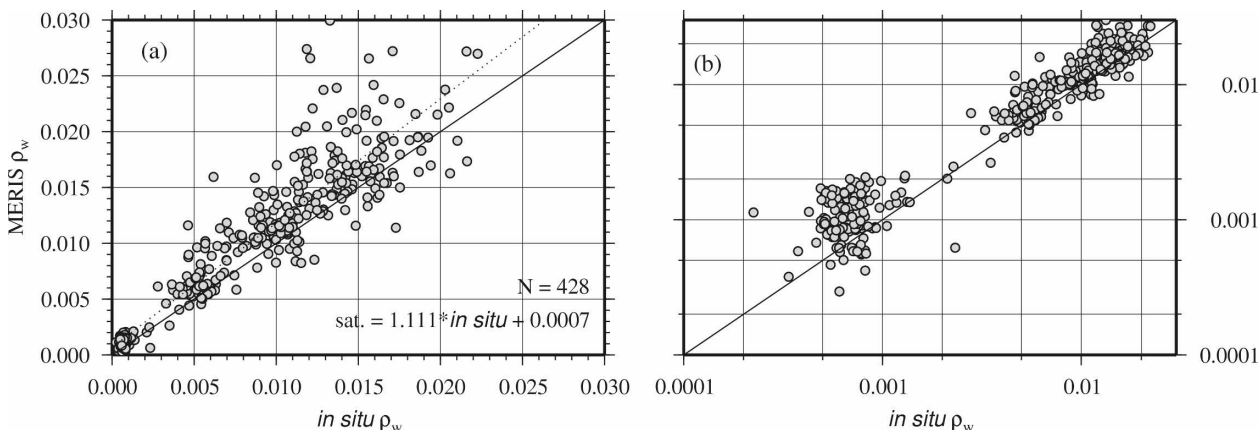


FIG. 16. (a), (b) An example of matchups between the water reflectances derived from the BOUSSOLE measurements and from satellite-borne ocean color observations (precisely from the European MERIS sensor here). All wavelengths are pooled together. Logarithmic scale for (a) is shown in (b) to magnify the low values in the red domain. The number of points and the coefficients of a linear regression are displayed in (a).

Although the present design and implementation basically fulfill the initial expectations, improvements are still desirable. They would require some additional engineering studies, and they are all focused toward improving the behavior of the buoy (i.e., minimizing the tilt due to swells and current). The lines along which improvements can be obtained are in (i) the use of lighter materials, such as carbon composites; (ii) the reduction of the instrumentation weight; and (iii) changes in the design itself. More significant modifications might be needed to adapt the design to other environments, for instance where currents are larger, or where significant tidally driven changes of the sea level occur.

An important characteristic of the BOUSSOLE buoy is its stability, which actually can serve a variety of applications that require a stable platform at sea. They include, for instance, measuring the atmospheric water vapor content using high-precision GPS systems coupled with a precise determination of the buoy position and movements, measuring the water level along the structure (measures of swells and waves, validation of radar altimetry measurements), and acoustic measurements in connection with deep-sea beacons.

APPENDIX

Mooring Line and Deployment Considerations

When the design of the BOUSSOLE buoy was initially proposed, some concerns arose as to whether it was reasonably feasible to deploy such a large structure over deep waters, having at the end the water level exactly positioned. This essentially means that an accuracy of a few tens of centimeters (less than 50 cm anyway) is needed on the total length of a mooring line that is about 2400 m in length. Having the buoy positioned too deep would increase exposure of the aerial instrumentation to sea spray and breaking waves. On the contrary, having too much of the superstructure above the sea level would modify the equilibrium of the platform, would increase the interaction between swells and the main buoyancy sphere, and could expose the upper arm to the risk of coming out of the water in harsh sea conditions (most certainly leading to breakage).

A specific deployment procedure was therefore set up. It includes two preliminary operations that are performed once and for all.

- 1) The first one consists of accurately measuring the water depth on the selected mooring site to determine the required length of all elements of the mooring line, all of them but the main Kevlar cable

being of predetermined dimensions (buoy, chains, acoustic releases, etc.). A margin is to be kept, so that the upper extremity of the Kevlar cable, after the cable has been elongated under the desired thrust, is at some depth greater than 20 m (i.e., the base of the buoy) but still reachable by divers using standard diving equipment. If the cable is too long, then the full procedure must be aborted because the cable cannot be shortened on site. If the depth is accurately known, the only remaining uncertainty is the number of meters the cable will stretch. An echo sounder survey was therefore conducted on the mooring site to provide the general topography of the sea bottom. The soundings were then calibrated into exact water depths thanks to several deep CTD casts, from which the measurement of the pressure (translated into depth using the simultaneous observations of temperature and salinity) was added to the measurement of an altimeter mounted on the CTD rosette (the CTD was stopped about 10 m before the bottom was reached). The water column thickness was, therefore, determined with accuracy <1 m.

- 2) The second critical and preliminary step consists of determining the cable length and its elongation under the tension of about 3 tons. The principle is first to weigh a sample of cable of a precisely known length (minimum of 20 m) with a high-precision balance, and then to adjust the length of the full mooring cable as a function of its total weight. This procedure proved to be robust, and is mandatory because the length counter used during the production of the cable is not accurate enough. The cable length must be computed so that it is at the desired length when under tension; the latter is estimated using a sample of the cable under production and the appropriate test bed for tension measurements.
- 3) Then, the course of the main operations for the deployment of the full mooring line (Fig. A1), which necessitates perfectly calm weather and a ship equipped with a dynamic positioning system, is as follow in numbers 4–12.
- 4) The mooring cable is uncoiled at the surface, starting from its “upper extremity” (the one that will be finally just below the buoy), while the ship heads to the mooring point at reduced speed. The cable is equipped at its extremity with a temporary length of rope terminated by a foam float.
- 5) The cable is fully deployed a few hundred meters before the ship reaches the mooring point, which reserves some time to deploy the next part of the mooring line (floatation spheres and acoustic re-

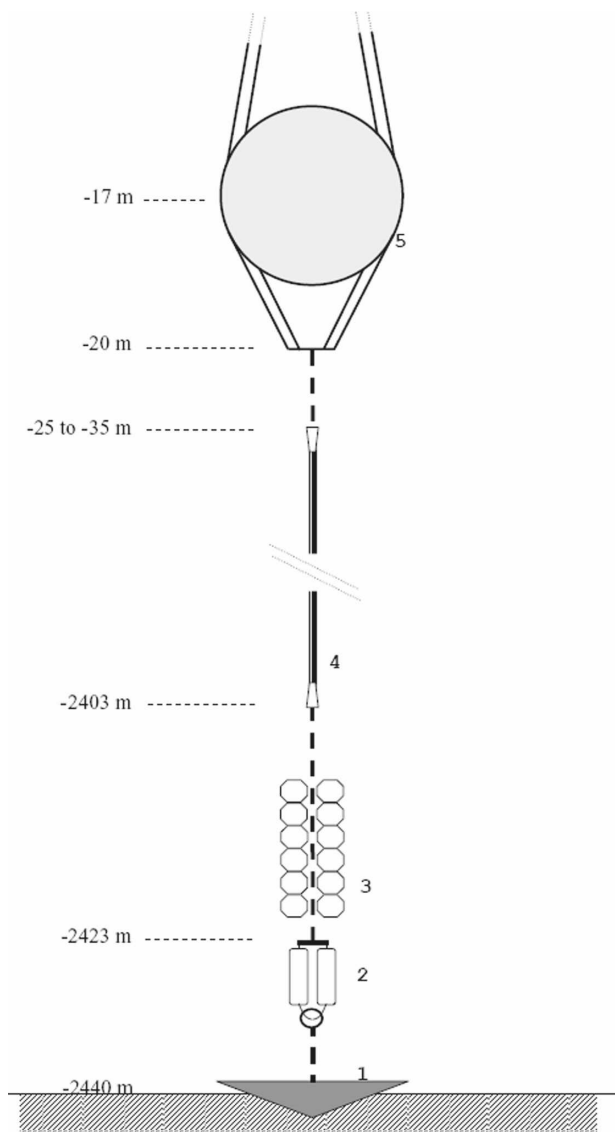


Figure A1. Simplified drawing of the mooring line; not to scale. The main elements are numbered as follows: 1) dead weight (5 tons in seawater, made of a pyramidal steel structure filled with a mixture of concrete and various steel scraps), 2) a pair of coupled acoustic releases (5-ton release load), 3) twelve Vitroflex floatation glass spheres protected in plastic shells (total buoyancy 3120 N), 4) 2330 m of neutrally buoyant Kevlar cable (diameter 14 mm; breaking point 12 tons), made of parallel Kevlar fibers coated into a polyurethane envelope, and equipped at each extremity with a galvanized steel termination, and 5) the buoy lower superstructure. Elements symbolized by dashed lines are segments of chain (also galvanized steel), the length of the one just below the buoy being adjusted during deployment while the other ones are predetermined before installation.

leases). Then, the only remaining part is the dead weight.

- 6) The dead weight is simply dropped in the water at about 100 m upstream of the mooring point, so that

it reaches this point when arriving at the sea floor after a rapid sink following a curved trajectory because of the drag of the cable.

- 7) The temporary foam float is then recovered aboard the ship and the cable is progressively put under the desired tension (i.e., about 3 tons) using a winch equipped with a strain gauge.
- 8) The lower buoy structure (the one with the sphere) is then lowered into the water by ballasting it with the appropriate weight, predetermined before departure on site. Once it is at the desired depth, divers connect it to the chain previously connected at the end of the cable. Two winches are needed during this step, where the dynamic positioning is also mandatory.
- 9) The tension applied to the cable by the winch is progressively released, simultaneously to the ballast being brought back aboard the ship. The buoy is therefore taking over from the winch to apply the 3-ton tension to the mooring cable. After this step is completed, the lower buoy structure is installed and ready to receive the upper superstructure.
- 10) The upper superstructure is laid down into the water. It is equipped with floats that are placed so that the buoy is vertical in the water, at about 1 m above its nominal water level.
- 11) Divers bring the section vertically above the lower part, and the connection is progressively obtained by trimming the buoyancy with underwater lift bags. The two parts are attached with simple stainless steel nuts and bolts. Note that all aluminum to steel contacts are isolated using appropriately shaped black Delrin pieces.
- 12) If needed, a final trim is performed either by lengthening or shortening the chain below the buoy. This can be done either by using a hoist or by reattaching some ballast to the buoy to slacken the cable. This operation might have to be repeated some time after the deployment, if current flow during the operation was pushing the buoy down and preventing the equilibrium water level from being reached.

The ideal sequence described above is usually perturbed by some unexpected event (change in weather, faulty parts, etc.), which is seemingly the rule when working at sea. Such anomalies occurred from time to time, but have never prevented the buoy from eventually and successfully being deployed.

Besides the full deployment procedure described above, a rotation of the upper superstructure is performed about every 6 months (twin buoys and instrument suites have been built), using a diving boat on site

and a helicopter for transportation of the superstructure from an onshore location to the offshore site and vice versa.

Acknowledgments. The BOUSSOLE project was established thanks to the work of numerous individuals, as well as the support and funding of several agencies and academic or governmental institutions. Specifically, the following contracts are acknowledged: the French Space Agency (CNES) provided funds after the project was evaluated by the Terre Océan Surfaces Continentales et Atmosphère (TOSCA) scientific committee, the European Space Agency (ESA) through the European Space Research and Technology Center (ESTEC) Contract 14393/00/NL/DC, the European Space Research Institute (ESRIN) through Contract 17286/03/I-OL, and the U.S. National Aeronautics and Space Administration (NASA) through a Letter of Agreement with the Université Pierre et Marie Curie, Paris 6. Stanford B. Hooker is specifically and warmly thanked for his help in establishing this agreement and for his unremitting support. The Institut National des Sciences de l'Univers (INSU) provides ship time for the monthly cruises. The cost of renting the engineering pool was taken by the Conseil Général du Var.

The crews and captains of the following ships are also warmly thanked for their help at sea: the *Castor-02* from the Fosevel Marine company (buoy and mooring operations), the INSU R/V *Tethys-II* (monthly servicing cruises), and the *GG-IX* from the Samar company (on-demand short operations on site). Pilots of the *Hélicoptères de France* helicopter company are also thanked for the survey missions above the BOUSSOLE site and transportation of the buoy upper superstructure to the mooring site.

Marc LeBoulluec, Yannick Aoustin, and Bernard Bigourdan, from the French institute IFREMER, and Øyvind Hellan, Bernt Leira, Rolf Barrholm, Svein Erling Heggelund, and Halvor Lie from the Norwegian company MARINTEK are also thanked for the engineering studies they performed in spring of 2002. Alpha Camara, from the *Avance Conceptuelle* Company, provided the final engineering design.

The data that are collected for several years near the BOUSSOLE site by the French weather forecast agency, Météo France, and are provided in near-real time on the Internet, have been of great help in the design and the analysis of the buoy behavior.

This paper is dedicated to the memory of one of our coauthors, Pierre Guevel, who died on 9 October 2007. He was a colleague and friend for over 20 years. He was the designer of the BOUSSOLE buoy and brought an invaluable contribution to the project.

REFERENCES

- Antoine, D., Ed., 2004: Guide to the creation and use of ocean colour, level-3, binned data products. Rep. Int. Ocean Color Coordinating Group 4, IOCCG, Dartmouth, Canada, 88 pp.
- , and Coauthors, 2006: BOUSSOLE: A joint CNRS-INSU, ESA, CNES and NASA ocean color calibration and validation activity. NASA Tech. Memo. TM-2006-214147, NASA GSFC, Greenbelt, MD, 59 pp.
- , F. D'Ortenzio, S. B. Hooker, G. Bécu, B. Gentili, D. Tailliez, and A. Scott, 2008: Assessment of uncertainty in the water-leaving reflectance determined by three satellite ocean color sensors (MERIS, SeaWiFS, MODIS-A) at an offshore site in the Mediterranean Sea (BOUSSOLE project). *J. Geophys. Res.*, in press.
- Argo Science Team, 1998: On the design and implementation of Argo—An initial plan for a global array of profiling floats. International CLIVAR Project Office ICPO Rep. 21, GODAE Rep. 5., GODAE International Project office, Melbourne, Australia, 32 pp.
- Bailey, S. W., and P. J. Werdell, 2006: A multi-sensor approach for the on-orbit validation of ocean color satellite data products. *Remote Sens. Environ.*, **102**, 12–23.
- Clark, D. K., H. R. Gordon, K. J. Voss, Y. Ge, W. Broenkow, and C. Trees, 1997: Validation of atmospheric correction over the oceans. *J. Geophys. Res.*, **102**, 17 209–17 217.
- , and Coauthors, 2003: MOBY, a radiometric buoy for performance monitoring and vicarious calibration of satellite ocean color sensors: Measurement and data analysis protocols. Ocean optics protocols for satellite ocean color sensor validation Rev. 4, Vol. VI, NASA Tech. Memo. 2003-211621, NASA GSFC, Greenbelt, MD, 141 pp.
- Dera, J., and H. R. Gordon, 1968: Light field fluctuations in the photic zone. *Limnol. Oceanogr.*, **13**, 697–699.
- Dickey, T., and Coauthors, 1998: Initial results from the Bermuda Testbed Mooring Program. *Deep-Sea Res.*, **45**, 771–794.
- Drinkwater, M. R., and Coauthors, 2005: The roadmap for a GMES operational oceanography mission. *ESA Bull.*, **124**, 43–48.
- Gordon, H. R., 1997: Atmospheric correction of ocean color imagery in the Earth Observing System era. *J. Geophys. Res.*, **102**, 17 081–17 106.
- , and K. Ding, 1992: Self-shading of in-water optical instruments. *Limnol. Oceanogr.*, **37**, 491–500.
- Graber, H. C., E. A. Terray, M. A. Donelan, W. M. Drennan, J. C. Van Leer, and D. B. Peters, 2000: ASIS—A new air–sea interaction spar buoy: Design and performance at sea. *J. Atmos. Oceanic Technol.*, **17**, 708–720.
- Gregg, W., Ed., 2007: Ocean-colour data merging. Rep. Int. Ocean Color Coordinating Group 6, IOCCG, Dartmouth, Canada, 68 pp.
- , and K. L. Carder, 1990: A simple spectral solar irradiance model for cloudless maritime atmospheres. *Limnol. Oceanogr.*, **35**, 1657–1675.
- Hellan Ø., B. Leira, R. Barrholm, S. Erling Heggelund, and H. Lie, 2002: Expert evaluation of Boussole buoy design. Marintek Rep. 700203.00:01, Trondheim, Norway, 46 pp.+appendices.
- Holben, B. N., and Coauthors, 1998: AERONET—A federated instrument network and data archive for aerosol characterization. *Remote Sens. Environ.*, **66**, 1–16.
- Hooker, S. B., and W. E. Esaias, 1993: An overview of the

- SeaWiFS Project. *Eos, Trans. Amer. Geophys. Union*, **74**, 241–246.
- , and C. R. McClain, 2000: The calibration and validation of SeaWiFS data. *Prog. Oceanogr.*, **45**, 427–465.
- , G. Zibordi, J. F. Berthon, D. D'Alimonte, S. Maritorena, S. McLean, and J. Sildam, 2001: Results of the second SeaWiFS data analysis round robin, March 2000 (DARR-00). NASA Tech. Memo 2001-206892, NASA GSFC, Greenbelt, MD, 71 pp.
- , C. R. McClain, and A. Mannino, 2007: NASA strategic planning document: A comprehensive plan for the long-term calibration and validation of oceanic biogeochemical data. NASA Special Publication SP-2007-214152, NASA GSFC, Greenbelt, MD, 31 pp.
- Hovis, W. A., and Coauthors, 1980: Nimbus-7 Coastal Zone Color Scanner: System description and initial imagery. *Science*, **210**, 60–63.
- LeBoulluec, M., Y. Aoustin, and B. Bigourdan, 2002: Expertise du flotteur Boussole. Rapport IFREMER TMSI/RED 02-028, Issy Les Moulineaux, France, 42 pp. + annexes.
- McClain, C. R., M. L. Cleave, G. C. Feldman, W. W. Gregg, S. B. Hooker, and N. Kuring, 1998: Science quality SeaWiFS data for global biosphere research. *Sea Technology*, *Compass*, 10–16.
- , S. B. Hooker, G. C. Feldman, and P. Bontempi, 2006: Satellite data for ocean biology, biogeochemistry and climate research. *Eos, Trans. Amer. Geophys. Union*, **87**, 337–343.
- Milburn, H. B., P. D. McClain, and C. Meining, 1996: ATLAS buoy—Reengineered for the next decade. *Proc. Oceans '96, Prospects for the 21st Century*, MTS/IEEE, 698–702.
- Millot, C., 1999: Circulation in the Western Mediterranean sea. *J. Mar. Syst.*, **20**, 423–442.
- Morel, A., and B. Gentili, 1993: Diffuse reflectance of oceanic waters. II. Bidirectional aspects. *Appl. Opt.*, **32**, 6864–6879.
- , and S. Maritorena, 2001: Bio-optical properties of oceanic waters: A reappraisal. *J. Geophys. Res.*, **106**, 7763–7780.
- Murphy, R. E., P. Ardanuy, F. J. DeLuccia, J. E. Clement, and C. F. Schueler, 2006: The Visible Infrared Imaging Radiometer (VIIRS). *Earth Science Satellite Remote Sensing*, J. J. Qu et al., Eds., Springer-Verlag and Tsinghua University Press, 199–223.
- Natvik, L. J., and G. Evensen, 2003: Assimilation of ocean colour data into a biochemical model of the North Atlantic. Part 1: Data assimilation experiment. *J. Mar. Syst.*, **40–41**, 127–153.
- O'Reilly, J. E., S. Maritorena, G. Mitchell, D. A. Siegel, K. L. Carder, D. L. Garver, M. Kahru, and C. R. McClain, 1998: Ocean color chlorophyll algorithms for SeaWiFS. *J. Geophys. Res.*, **103**, 24 937–24 950.
- Pinkerton, M., and J. Aiken, 1999: Calibration and validation of remotely sensed observations of ocean color from a moored data buoy. *J. Atmos. Oceanic Technol.*, **16**, 915–923.
- Rast, M., J. L. Bézy, and S. Bruzzi, 1999: The ESA Medium Resolution Imaging Spectrometer MERIS—A review of the instrument and its mission. *Int. J. Remote Sens.*, **20**, 1681–1702.
- Salomonson, V. V., D. L. Toll, and W. T. Lawrence, 1992: Moderate resolution imaging spectroradiometer (MODIS) and observations of the land surface. *Proc. Int. Geoscience and Remote Sensing Symp.*, Houston, TX, IGARSS, 549–551.
- Sathyendranath, S., Ed., 2000: Remote sensing of ocean colour in coastal, and other optically-complex, waters. Rep. Int. Ocean Color Coordinating Group 3, IOCCG, Dartmouth, Canada, 140 pp.
- Shettle, E. P., and R. W. Fenn, 1979: Models for the aerosols of the lower atmosphere and the effects of humidity variations on their optical properties. Environmental Research Papers 676, AFGL-TR-79-0214, Air Force Geophysics Laboratory, Hanscom AFB, Massachusetts, 31 pp.
- Stramska, M., and T. D. Dickey, 1998: Short-term variability of the underwater light field in the oligotrophic ocean in response to surface waves and clouds. *Deep-Sea Res. I*, **45**, 1393–1410.
- Walker, R. E., 1994: *Marine Light Field Statistics*. Wiley, 675 pp.
- Yoder, J. A., Ed., 1999: Status and plans for satellite ocean-colour missions: Considerations for complementary missions. Rep. Int. Ocean-Colour Coordinating Group 2, IOCCG, Dartmouth, Canada, 43 pp.
- Zaneveld, J. R. V., E. Boss, and A. Barnard, 2001: Influence of surface waves on measured and modeled irradiance profiles. *Appl. Opt.*, **40**, 1442–1449.
- Zibordi, G., J.-F. Berthon, J. P. Doyle, S. Grossi, D. van der Linde, C. Targa, and L. Alberotanza, 2002: Part 1: A tower-based long-term measurement program, Coastal Atmosphere and Sea Time Series (CoASTS). NASA Tech. Memo. 2002–206892, Vol. 19, NASA Goddard Space Flight Center, 29 pp.
- , D. D'Alimonte, and J.-F. Berthon, 2004: An evaluation of depth resolution requirements for optical profiling in coastal waters. *J. Atmos. Oceanic Technol.*, **21**, 1059–1073.
- , and Coauthors, 2006a: A network of standardized ocean color validation measurements. *Eos, Trans. Amer. Geophys. Union*, **87**, 293–304.
- , F. Mélin, and J.-F. Berthon, 2006b: Comparison of SeaWiFS, MODIS and MERIS radiometric products at a coastal site. *Geophys. Res. Lett.*, **33**, L06617, doi:10.1029/2006GL025778.